BIOCHEMISTRY
including biophysical chemistry & molecular biology
Article

Biochemistry **2010,** *49,* 1005–1013 1005
DOI: 10.1021/bi9019737

Nucleotide- and Substrate-Induced Conformational Transitions in the CBS Domain-Containing Pyrophosphatase of *Moorella thermoacetica*[†]

Joonas Jämsen,[‡] Alexander A. Baykov,*[,§] and Reijo Lahti*[,‡]

[‡]*Department of Biochemistry and Food Chemistry, University of Turku, FIN-20014 Turku, Finland and* [§]*A. N. Belozersky Institute of Physico-Chemical Biology, Moscow State University, Moscow 119899, Russia*

Received November 16, 2009; Revised Manuscript Received December 28, 2009

ABSTRACT: In contrast to all other known pyrophosphatases, *Moorella thermoacetica* pyrophosphatase (*mt*CBS-PPase) contains nucleotide-binding CBS domains and is thus strongly regulated by adenine nucleotides. Stopped-flow measurements using a fluorescent AMP analogue, 2′(3′)-*O*-(*N*-methylanthranoyl)-AMP (Mant-AMP), reveal that nucleotide binding to *mt*CBS-PPase involves a three-step increase in Mant-AMP fluorescence with relaxation times from 0.01 to 100 s, implying conformational changes in the complex. This effect is reversed by AMP. Metal cofactors (Co^{2+} and Mg^{2+}) enhance the fluorescence signal but are not absolutely required, unlike what is seen when the catalytic reaction is examined. The relaxation times and amplitudes of the fluorescence signals depend on Mant-AMP concentration in a manner suggestive of the presence of a second binding site for Mant-AMP on the protein. Equilibrium fluorescence titration experiments additionally support the presence of two types of AMP binding sites with different affinities, whereas equilibrium dialysis and membrane filtration measurements reveal binding of one AMP molecule per enzyme monomer, implying negative cooperativity in nucleotide binding. The substrate (PP_i) modulates Mant-AMP binding, leading to a further conformational change in the enzyme−Mant-AMP complex, and stimulates *mt*CBS-PPase in alkaline medium within a time scale of minutes, via conversion to a more active form. This active form initially comprises only a third of the enzyme, as estimated from kinetic titration with ADP. AMP inhibits both enzyme forms but is unable to independently induce interconversion. Our results collectively suggest that nucleotides and the substrate induce multiple conformational changes in *mt*CBS-PPase occurring over a wide time scale; the changes are distinct and almost independent.

Inorganic pyrophosphate (PP_i) is formed in vast quantities as a byproduct of biosynthetic reactions, including protein, RNA, and DNA syntheses. The PP_i concentration in turn affects the equilibria of these important physiological reactions (*1*). In *Bacilli*, *Clostridia*, and other bacterial lineages, including several human pathogens, the intracellular level of PP_i is controlled by family II pyrophosphatase (PPase,[1] EC 3.6.1.1) that catalyzes conversion of PP_i to P_i. Unlike compact one-domain family I PPases (*2*), family II PPases contain two well-defined domains connected by a flexible linker (*3*, *4*). As the active site is located between the domains, this structural organization is well suited for the allosteric regulation of PPase activity. Indeed, the N-terminal domains of approximately a quarter of known family II PPase sequences contain a large insert (∼100−125 residues) comprising two CBS domains forming a Bateman fold (*5*). This structure, originally found in cystathionine β-synthase (*5*), binds regulatory adenine nucleotides and is found in a variety of proteins from all kingdoms of life (*6*, *7*). We have recently expressed and isolated a CBS domain-containing PPase of *Moorella thermoacetica* (*mt*CBS-PPase). In contrast to all other known PPases, the enzyme is regulated by adenine nucleotides (*8*). The direction of the effect depends on the nucleotide used (inhibition by AMP and ADP and activation by ATP), and binding affinities for the nucleotides are in the submicromolar range.

CBS domains usually occur as tandem repeats in proteins and are independent folding units that retain their structure and binding properties, even when separated from the bulk protein (*7*). These domains bind adenine nucleotides with varying affinities and thus act as sensors of cellular energy status (*6*, *7*). More recently, CBS domains have been implicated in the control of intracellular trafficking of chloride channel ClC-5 (*9*); gating of osmoregulatory transporter OpuA, via osmotic strength (*10*, *11*); Mg^{2+} transfer by the transporter MgtE (*12*); plant vacuolar nitrate transport by the transporter AtCLCa (*13*); and adenylate nucleotide synthesis (*14*). Interestingly, substitution of conserved residues in CBS domains impairs nucleotide regulation of specific proteins and triggers a variety of human hereditary diseases (*6*, *7*). The three-dimensional structures of several CBS domain-containing proteins or their individual CBS domain regions have recently been published (*15*−*22*). However, the structures of both nucleotide-bound and nucleotide-free forms have not been established for any particular protein, and the structural basis for activity regulation by CBS domains remains to be elucidated.

[†]This work was supported by Academy of Finland Grant 114706, Russian Foundation for Basic Research Grant 09-04-00869, and a grant from the Ministry of Education and the Academy of Finland (for the National Graduate School in Informational and Structural Biology).

*To whom correspondence should be addressed. R.L.: telephone, 358-2-333-6845; fax, 358-2-333-6860; e-mail, reijo.lahti@utu.fi. A.A.B.: telephone, 7-495-939-5541; fax, 7-495-939-3181; e-mail, baykov@genebee.msu.su.

[1]Abbreviations: CBS, cystathionine β-synthase; DTPA, diethylenetriaminepentaacetic acid; Mant-AMP, 2′(3′)-*O*-(*N*-methylanthranoyl)adenosine 5′-monophosphate; *mt*CBS-PPase, CBS domain-containing PPase from *M. thermoacetica*; PPase, inorganic pyrophosphatase.

Published on Web 12/28/2009

In many respects, *mt*CBS-PPase resembles common family II PPases that lack CBS domains. Specifically, *mt*CBS-PPase requires a transition metal cofactor for activity and is maximally active in the presence of both Co^{2+} and Mg^{2+}. Co^{2+} or Mn^{2+} alone is less effective, whereas Mg^{2+} alone confers only negligible activity (*8*). The enzyme is a homodimer of 48.1 kDa subunits (436 residues), which partially dissociates in the absence of divalent metals (*8*). Except for the CBS domain-containing insert (~125 residues), the amino acid sequence of *mt*CBS-PPase is similar to those of common family II PPases and contains all 13 conserved active site residues identified using X-ray crystallography (*3*, *4*). The most striking differences between *mt*CBS-PPase and common family II PPases include sensitivity to adenine nucleotides and a 1000-fold lower activity. It is hypothesized that the CBS domain insert acts as an "internal inhibitor" of *mt*CBS-PPase, sensitizing enzyme activity to structural changes caused by nucleotide binding to this domain and consequently facilitating further inhibition or activation (*8*). In the framework of this hypothesis, AMP and ADP enhance whereas ATP partially compensates for the effect of the CBS insert.

Here, we employ different kinetic and binding measurement techniques to characterize and compare the conformational transitions in *mt*CBS-PPase induced by binding of AMP and its fluorescent analogue, Mant-AMP, to CBS domains, as well as to explore substrate binding to the active site.

EXPERIMENTAL PROCEDURES

Reagents. AMP (free acid) and ADP (potassium salt) were obtained from Fluka, and Mant-AMP (trimethylammonium salt) was from Jena Bioscience. The concentrations of nucleotide stock solutions were estimated by measuring absorbance at 259 nm (ε = 15900 M^{-1} cm^{-1}). [^{14}C]AMP was acquired from Moravek Radiochemicals, and the NanoOrange protein assay kit was from Invitrogen. All other reagents and kits were from Sigma.

mtCBS-PPase. Expression and purification of electrophoretically homogeneous *mt*CBS-PPase were performed as described previously (*8*), with some modifications. Na^+ was replaced with K^+ in all buffers due to a somewhat higher yield and specific activity of the final preparation observed with the latter ion. Gel filtration was performed in 50 mM MOPS-KOH (pH 7.2) with 5 mM $MgCl_2$, 0.1 mM $CoCl_2$ and 20 μM DTPA. Combined protein fractions were concentrated to approximately 120 mg/mL using a Centricon YM-10 centrifugal filter device (Amicon) with a 10 kDa cutoff membrane, frozen in liquid nitrogen, and stored at −70 °C. Dilutions were prepared with MOPS-KOH buffer containing $MgCl_2$ and $CoCl_2$, but no DTPA. Where required, metals were removed from enzyme samples by treatment overnight in 50 mM MOPS-KOH (pH 7.2), with 2 mM DTPA. DTPA was subsequently removed by dialysis against buffer without DTPA.

Concentrations of *mt*CBS-PPase solutions were determined on the basis of a specific absorption coefficient ($A^{1\%}_{280}$) of 4.8, calculated from the amino acid composition using ProtParam, and verified by direct weighing of protein samples after dehydration in a vacuum oven (*23*). The *mt*CBS-PPase concentrations obtained were consistent with those reported with the NanoOrange protein assay (*24*) using bovine serum albumin as the standard. Molar concentrations of *mt*CBS-PPase were calculated using a subunit molecular mass of 48.1 kDa.

The possible presence of tightly bound ADP in *mt*CBS-PPase was assessed by measuring the effects of incubation of a stock enzyme solution for up to 24 h with pyruvate kinase and phosphoenolpyruvate on *mt*CBS-PPase activity. This treatment was expected to convert bound ADP (inactive enzyme) into ATP (active enzyme). On the basis of the lack of activation, *mt*CBS-PPase was judged as ADP-free.

Activity Measurements. The assay medium (total volume of 25 mL) contained 0.1 M MOPS-KOH (pH 7.2), 5 mM $MgCl_2$, 0.1 mM $CoCl_2$ (hereafter termed assay buffer), and 0.16 mM PP_i, except where specified otherwise. The reaction was initiated via addition of 5−150 μL of a diluted enzyme solution, leading to a final enzyme concentration of 0.02−2 μg/mL. P_i formation was monitored at 25 °C for 8−25 min using an automatic P_i analyzer (*25*). The buffers employed in pH studies included acetic acid-KOH (pH 5) or TAPS-HCl (pH 8 and 8.5) at a concentration of 0.1 M.

Stopped-Flow Measurements. Time-resolved fluorescence measurements of binding of Mant-AMP to *mt*CBS-PPase were performed on the Applied Photophysics model SX.18MV stopped-flow spectrofluorometer. For measurement of changes in Mant-AMP emission upon excitation of protein tryptophan, the excitation wavelength was set at 295 nm and emission detected using a Schott GG400 filter at >400 nm. The dead time of the instrument, determined from reduction of 2,6-dichlorophenolindophenol by L-ascorbic acid, was 1.5 ms (*26*). Monochromator slits were set at 2 nm, and the temperature of operation was 22 ± 1 °C. The final enzyme concentration was 2.5 μM in all experiments, and the Mant-AMP concentration varied within the range of 4−250 μM. Equal volumes of the two solutions were mixed in all cases, and fluorescence was monitored for 500 s.

Static Fluorescence Measurements. Intrinsic protein fluorescence was excited at 295 nm, and emission spectra were captured by scanning at 305−600 nm on a Varian Cary Eclipse spectrofluorometer (Varian Inc.) in a 90° mode with excitation and emission slits set to 5 nm. Mant-AMP fluorescence was excited at 355 nm and measured at 375−600 nm. The temperature was maintained at 25 °C using a Peltier accessory with magnetic stirring, except where specified otherwise. The enzyme concentration in spectral titrations was 1 μM, taking the effect of dilution with a nucleotide solution (<10%) into account. Mixtures were incubated for 5 min after each nucleotide addition, prior to measurement. Measured fluorescence values were corrected for any additional fluorescence imposed by the nucleotides and inner filter effect.

Filtration Binding Measurements. AMP binding to *mt*CBS-PPase was assessed on Millipore Multiscreen 96-well filtration plates with an IP membrane (Millipore Corp.). The membrane was prewashed once with 20% ethanol and three times with the assay buffer. A protein solution (10 μM, 0.1 mL volume) prepared with the same buffer was added to the plate chambers for 10 min, followed by 50 μL of ^{14}C-labeled AMP (200−5000 cpm). The binding reaction was allowed to proceed for 5 min at 25 °C, after which vacuum was applied to the plates to empty the chambers in approximately 1 s. Each filter was washed twice with 100 μL of assay buffer. Controls run in parallel contained bovine serum albumin in lieu of *mt*CBS-PPase. The radioactivity of the filter was determined in the liquid scintillation cocktail, Ultima Gold XR (0.2 mL), with a Hidex Chameleon V multimode microplate reader (Hidex Ltd.). The variation between series in this binding assay was <8%.

Equilibrium Dialysis. The single-use DispoEquilibrium Dialyzer (Harvard Apparatus) was employed to measure binding of [^{14}C]AMP to *mt*CBS-PPase. Each chamber initially contained

40 μL of assay buffer with 0.15 M KCl and 0.1−50 μM ^{14}C-labeled AMP. One chamber additionally contained 10 μM *mt*CBS-PPase. Equilibration of samples was achieved in 4.5 h (empirically determined), followed by centrifugal separation. The recovered volumes of solution from each chamber were measured and 5 μL aliquots withdrawn to determine enzyme activity using a BioMol Green phosphate assay kit (Enzo Life Sciences International Inc.) and protein concentration with the NanoOrange protein assay kit. No appreciable inactivation of *mt*CBS-PPase was observed during dialysis. Finally, 1 mL of Ultima Gold XR was added, and the radioactivity in both chambers was determined with a liquid scintillation counter.

Data Analyses. All nonlinear least-squares fittings were performed with SCIENTIST (MicroMath). Fluorescence titration data were analyzed in terms of Scheme 1, where E is the *mt*CBS-PPase dimer, N is AMP, and EN and EN_2 represent their complexes. The values for the dissociation constants, K_{d1} and K_{d2}, and the ratio of fluorescence changes due to EN and EN_2 formation (a) were obtained by simultaneously fitting eqs 1−5 to the dependencies of the measured fluorescence changes, ΔF, on total AMP concentration $[N]_0$ with SCIENTIST.

$$\Delta F = \Delta F_{max}(a[EN] + [EN_2])/[E]_0 \quad (1)$$

$$[E][N]/[EN] = K_{d1} \quad (2)$$

$$[EN][N]/[EN_2] = K_{d2} \quad (3)$$

$$[E] + [EN] + [EN_2] = [E]_0 \quad (4)$$

$$[N] + [EN] + 2[EN_2] = [N]_0 \quad (5)$$

In these equations, ΔF_{max} represents the fluorescence change for fully bound *mt*CBS-PPase and [N] is the free AMP concentration. This treatment takes into account the decrease in free AMP and free enzyme concentrations due to complex formation. Equations 2 and 3 define the binding constants, while eqs 4 and 5 describe mass conservation for *mt*CBS-PPase and AMP.

The relaxation times and amplitudes for stopped-flow fluorescence traces were determined with eq 6

$$F = F_{lim} - \sum_{i=1}^{n} F_i e^{-t/\tau_i} \quad (6)$$

where F and F_{lim} are the fluorescence intensities at time t and infinity, respectively, F_i is the amplitude and τ_i the relaxation time for the ith relaxation process, and n represents the relaxation process number. The dependence of relaxation times on nucleotide concentration was fit to eq 7:

$$1/\tau_i = 1/\tau_{i,lim} + (1/\tau_{i,0} - 1/\tau_{i,lim})/(1 + [N]/K_d) \quad (7)$$

where $\tau_{i,0}$ and $\tau_{i,lim}$ are the relaxation times at zero and infinite nucleotide concentrations, respectively, and K_d is the dissociation constant for the enzyme−nucleotide complex. Amplitude dependence was analyzed with eq 8 or its alternative form (eq 9), which implies that the amplitude increases upon nucleotide binding but decreases nonspecifically at high nucleotide concentrations. $F_{i,lim}$ is the limiting value of the amplitude, and α is a constant referring to the nonspecific effect of the nucleotide.

$$F_i = F_{i,lim}/(1 + [N]/K_d) \quad (8)$$

$$F_i = F_{i,lim}/(1 + K_d/[N] + \alpha[N]) \quad (9)$$

Scheme 1: Nucleotide Binding to *mt*CBS-PPase

$$E \overset{K_{d1}}{\leftrightarrow} EN \overset{K_{d2}}{\leftrightarrow} EN_2$$

Time courses of PP_i hydrolysis were fit to eqs 10 and 11, where A_0, A, and A_{lim} are maximal velocities at time zero, t, and infinity, respectively, $[E]_0$ is the total enzyme concentration, k is the first-order rate constant for transition between inactive and active enzyme forms, and K_m is the Michaelis constant. Equation 11 assumes that activity increases or decreases due to enzyme transition between two states and decreases upon substrate depletion. The values of A_0, A_{lim}, and k were treated as adjustable parameters. The K_m value, initially set at 10 μM at the initial round of calculation, was subsequently estimated from the calculated dependencies of A_0 and/or A_{lim} on $[S]_0$, and the calculation cycle repeated with the refined K_m value until the results converged.

$$d[P]/dt = A[E]_0 \quad (10)$$

$$A = [A_0 + (A_{lim} - A_0)(1 - e^{-kt})](1 + K_m/[S]_0)/[1 + K_m/([S]_0 - [P])] \quad (11)$$

RESULTS

Equilibrium Mant-AMP and AMP Binding. The relatively low intrinsic fluorescence of *mt*CBS-PPase was not significantly altered upon AMP binding. We additionally examined a fluorescent analogue, Mant-AMP, in which an *N*-methylanthranoyl group is attached through the 2′- or 3′-ribose oxygen (*27*), to monitor nucleotide binding to *mt*CBS-PPase. The excitation spectrum of Mant-AMP, containing a peak at 355 nm, and the emission spectrum of protein Trp residues largely overlap, resulting in very efficient energy transfer between Trp and Mant-AMP. This facilitates excitation of Mant-AMP fluorescence at the Trp peak (295 nm), ensuring considerably lower background fluorescence from nonbound Mant-AMP, compared with excitation at 355 nm. Accordingly, fluorescence titration was performed using Trp excitation (295 nm) and emission monitored at 455 or 342 nm in Mant-AMP or AMP binding measurements, respectively.

The binding profile of Mant-AMP (Figure 1A) suggests the presence of two types of binding sites with different K_d values (Table 1), as estimated by fitting of eqs 1−5. The one-site model exhibited a markedly poorer fit, which was further emphasized by the distribution of residuals (top panels in Figure 1). The binding profile for AMP was less precise, as the intrinsic fluorescence of *mt*CBS-PPase was low and did not change significantly upon AMP binding. However, the two-site model (Scheme 1) was superior in terms of fit quality with AMP. The binding constants, K_{d1} and K_{d2}, showed pairwise similarity between Mant-AMP and AMP (Table 1). Factor a in eq 1 was estimated to be 0.24 ± 0.03 for both nucleotides, indicating that formation of EN_2 caused an approximately 4-fold greater increase in fluorescence, compared with EN formation.

Rapid Kinetics of Mant-AMP Binding. The stopped-flow technique was employed to resolve Mant-AMP binding in time. Upon mixing of *mt*CBS-PPase with Mant-AMP (final concentration of 250 μM) in the stopped-flow instrument, we observed a series of Mant-AMP fluorescence changes (Figure 2A). Computer analysis of the traces revealed three relaxation processes with

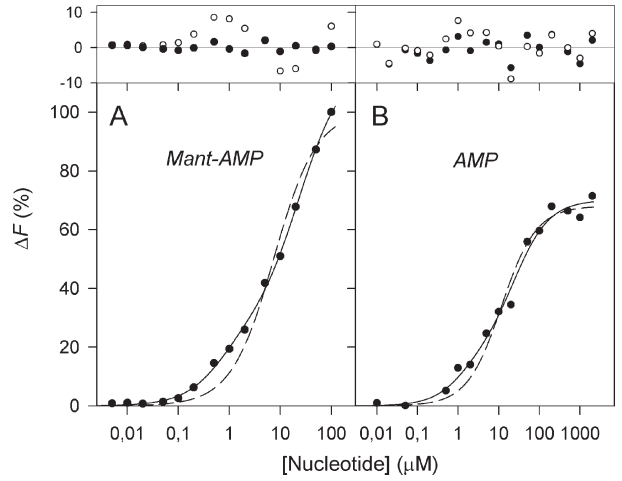

FIGURE 1: Fluorescence titration of nucleotide-binding sites in *mt*CBS-PPase with Mant-AMP (A) and AMP (B). Excitation and emission wavelengths were 295 and 470 nm for Mant-AMP and 295 and 342 nm for AMP, respectively. The solid and dashed lines represent the best fits for eqs 1−5 with two binding sites and one binding site, respectively (in the latter case, K_{d2} was set to infinity). The top panels depict the distribution of residuals for the solid (●) and dashed (○) lines.

Table 1: Dissociation Constants for Nucleotide Binding to Free Enzyme Derived from Equilibrium Measurements

nucleotide	method	K_{d1} (μM)	K_{d2} (μM)
AMP	fluorescence titration	1.2 ± 0.8	25 ± 10
Mant-AMP	fluorescence titration	0.6 ± 0.1	24 ± 3
AMP	equilibrium dialysis		16 ± 5
AMP	membrane filtration		11 ± 4

relaxation times (τ) of 0.023, 4.5, and 240 s, leading to increased Mant-AMP fluorescence. The relative amplitude values for these processes were 1.0, 1.1, and 8.6, respectively. No signals were detected when either enzyme or Mant-AMP was omitted from the solutions prior to mixing.

When the binding reaction was performed in the presence of 250 μM PP_i (added along with Mant-AMP), the stopped-flow traces exhibited several significant changes (Figure 2B). The fluorescence initially increased to a level exceeding that observed in the absence of PP_i (Figure 2A) followed by a decrease to that level. The latter effect is clearly attributable to PP_i depletion, which is hydrolyzed by *mt*CBS-PPase under the conditions employed. The number of detectable relaxation processes in the ascending part of the curve decreased to two, with relaxation times of 0.033 and 20 s. The former relaxation time is close to τ_1 measured in the absence of PP_i, whereas the latter time is intermediate between τ_2 and τ_3 and differs significantly from both. These findings suggest that PP_i binding induces changes in the enzyme, leading to increases in both the rate and amplitude of the fluorescence signal elicited by Mant-AMP binding.

Addition of excess AMP to the preformed enzyme−Mant-AMP complex led to elimination of Mant-AMP fluorescence (Figure 2C) because of the displacement of bound Mant-AMP. This back transition occurred in two steps, with τ values of 0.85 and 20 s and relative amplitudes of 1.0 and 5.9, respectively.

Effect of Mant-AMP Concentration on Binding Kinetics. Surprisingly, inverse relaxation times for all three of the processes observed in Figure 2A decreased in a saturatable manner

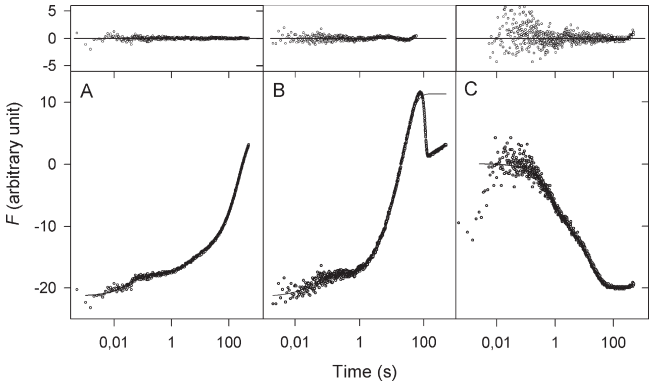

FIGURE 2: Fluorescence stopped-flow kinetic traces. (A) Mant-AMP binding upon mixing 5 μM *mt*CBS-PPase and 500 μM Mant-AMP solutions in assay buffer. (B) Effect of PP_i on Mant-AMP binding traces. The enzyme solution (2 μM) was combined with a mixture of 125 μM Mant-AMP and 500 μM PP_i. (C) Reversal of enzyme-bound Mant-AMP fluorescence by AMP. An enzyme solution (5 μM) pre-equilibrated with 30 μM Mant-AMP was combined with a mixture of 250 mM AMP and 30 μM Mant-AMP (added to maintain the Mant-AMP concentration over the course of the experiment). Fluorescence signals in all panels were normalized to the same enzyme concentration. Excitation was at 295 nm, while emission was monitored at > 400 nm. The abscissa shows the times after mixing components in the stopped-flow instrument. The lines represent the best fits for the three-exponential (A) or two-exponential (B and C) form of eq 6. For panel B, only the initial part of the curve (< 60 s) was fitted. The top panels show distribution of residuals of the fits.

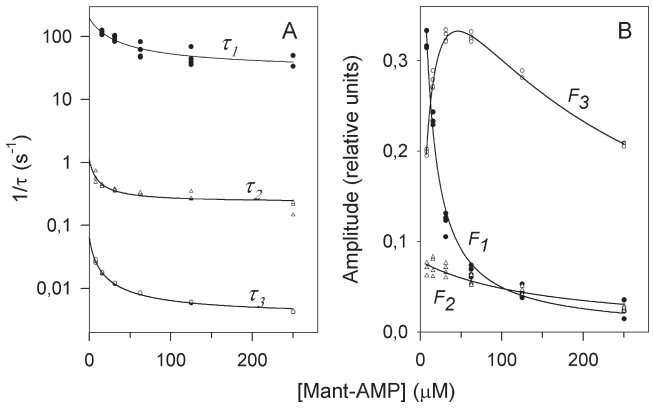

FIGURE 3: Dependence of the reciprocals of the relaxation times (A) and amplitudes (B) describing binding of Mant-AMP to *mt*CBS-PPase at different nucleotide concentrations. The abscissa depicts the total nucleotide concentration minus the nucleotide concentration bound to the fluorescence-inducing binding [2.5 μM (Results)]. Conditions were similar to those described in the legend of Figure 2. The lines depict the best fit for eq 7 (A), eq 8 (B, dependence of F_1), or eq 9 (B, dependence of F_3).

with an increase in Mant-AMP concentration (Figure 3). This finding indicates that none of the relaxation processes correspond to a second-order reaction of Mant-AMP binding to *mt*CBS-PPase, in which the inverse relaxation time should increase linearly with Mant-AMP concentration. Thus, the binding step proceeded faster than did all the transitions detected in Figure 2. Furthermore, the dependencies shown in Figure 3A suggest that Mant-AMP additionally binds to a modulatory site, which occurs faster than the transitions displayed in panels A and B of Figure 2. Fitting the dependencies for τ_1, τ_2, and τ_3 in Figure 3A to eq 7 yielded the parameter values listed in Table 2. Notably, K_d values for the modulatory site derived from τ_1, τ_2, and τ_3 dependencies were similar (approximately 10 μM), within the error of determination.

Table 2: Parameter Values in eq 2 Derived from Stopped-Flow Measurement of Mant-AMP Binding

dependence analyzed	$\tau_{i,0}$ (s)	$\tau_{i,\mathrm{lim}}$ (s)	K_d[a] (μM)
τ_1	0.005 ± 0.001	0.03 ± 0.01	20 ± 13 (11 ± 2)
τ_2	0.9 ± 0.4	4.4 ± 0.4	8 ± 5
τ_3	23 ± 2	280 ± 20	7 ± 1 (13 ± 2)

[a] K_d values shown in parentheses were estimated from F_i dependencies (Figure 2B) with eqs 8 and 9.

The amplitude for the fastest relaxation process (F_1) decreased hyperbolically with an increasing Mant-AMP concentration (Figure 3B), yielding a similar K_d value of 11 μM, when eq 8 was employed. F_3 was increased at low and reduced at high nucleotide concentrations. A similar decline was observed for the F_2 dependence. This was an instrumental effect, presumably arising during the mixing step within the stopped-flow apparatus, as no decline in fluorescence (which is actually the sum of F_1, F_2, and F_3) was observed upon fluorescence titration (Figure 1A). The instrumental effect may also contribute to the F_1 dependence; however, the estimated K_d value increased insignificantly when the F_1 dependence was analyzed with eq 9 using the α value derived from the F_3 dependence. The K_d value derived from the ascending part of the F_3 dependence was 13 μM. The results of amplitude analyses thus support the presence of the modulatory site deduced from τ analysis. The amplitude for the "instant" binding step could not be estimated in the experiments shown in Figure 2, as the initial fluorescence level was not fixed, and the final fluorescence level was employed as the reference point. However, we observed no significant instant changes in fluorescence attributable to formation of the enzyme−Mant-AMP complex in separate runs in which Mant-AMP was mixed with buffer, enzyme with buffer, and, finally, Mant-AMP with enzyme, at Mant-AMP concentrations of 4−16 μM, which is sufficient for the occupation of both binding sites.

Metal Cofactor Requirements of Mant-AMP-Induced Transitions. *mt*CBS-PPase is inactive in the absence of the metal cofactor, slightly activated by Mg^{2+}, substantially activated by Co^{2+}, and maximally active in the presence of both Co^{2+} and Mg^{2+} (*8*). In our experiments, these metal ions affected the rate and magnitude of Mant-AMP-induced fluorescence changes but were not absolutely required. Binding of Mant-AMP to the metal-depleted enzyme also involved three steps; however, steps 2 and 3 proceeded at higher (3−12-fold) rates, and a 3.6-fold lower amplitude was observed in step 3 (Table 3). Co^{2+} alone accelerated steps 1 (3.5-fold) and 2 (13-fold) and induced a 1.7-fold increase in A_3. Further addition of Mg^{2+} led to deceleration of all steps (2−150-fold) and increased the amplitude of step 3.

Direct Measurements of AMP Binding. The stoichiometry of binding of ^{14}C-labeled AMP to *mt*CBS-PPase was measured using equilibrium dialysis and membrane filtration techniques (Figure 4). Within the error of measurements, binding profiles were described well by the single-site model, with K_d values similar to the K_{d2} values obtained in the fluorescence titrations depicted above (Figure 1 and Table 1). A main problem is the rather low precision inherent in dialysis and filtration methods. Thus, we could not detect heterogeneity of binding sites and used a one-site binding model for analysis. Most importantly, the binding stoichiometry was 1.1 ± 0.1 mol/mol of subunit in the dialysis assay and 0.66 ± 0.07 mol/mol of subunit in the filtration assay. The lower value obtained with the latter method may be explained by partial dissociation of the complex during the washing step. A nucleotide binding stoichiometry of 1 mol/mol of subunit has been reported from the X-ray structures of *Clostridia perfringens* PPase (H. Tuominen, E. Oksanen, and R. Lahti, unpublished work) and other CBS proteins (*15*, *17*, *19*, *22*), although all these proteins contain a pair of CBS domains per subunit, similar to *mt*CBS-PPase.

Table 3: Cofactor Dependence of the Kinetic Parameters for Mant-AMP Binding[a]

parameter	Co and Mg	Co	no cofactor
A_1	164 ± 15	123 ± 3	161 ± 37
A_2	44 ± 3	55 ± 21	30 ± 3
A_3	368 ± 40	173 ± 20	101 ± 5
τ_1 (s)	0.0245 ± 0.002	0.0045 ± 0.0012	0.0158 ± 0.0045
τ_2 (s)	11.6 ± 3.5	0.075 ± 0.022	0.96 ± 0.3
τ_3 (s)	156 ± 12	80 ± 10	51 ± 5

[a] Measured at a final Mant-AMP concentration of 125 μM. Cofactors, where indicated, were 0.1 mM Co^{2+} and 5 mM Mg^{2+}.

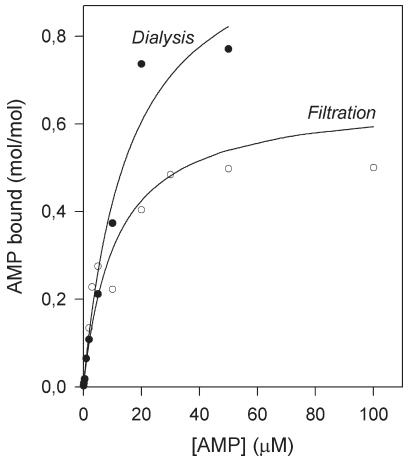

FIGURE 4: Stoichiometry of binding of AMP to *mt*CBS-PPase determined with equilibrium dialysis (●) and membrane filtration (○). The abscissa depicts the concentration of free unbound AMP, which was directly measured (dialysis) or calculated as the difference between total and bound AMP concentrations (filtration). The lines represent the best fits for a simple hyperbolic function.

No changes in AMP binding (100 μM) were observed upon omission of Co^{2+} and Mg^{2+} from the reaction medium using the filtration technique. These data suggest that metal cofactors are not required for nucleotide binding.

Activity Transition during Catalysis. A slow transition of *mt*CBS-PPase induced by PP_i was detected using steady-state activity measurements. The initial sections of the progress curves for steady-state PP_i hydrolysis (reaction time of < 5 min) in the absence of nucleotides were nonlinear at PP_i concentrations in excess of the respective K_m values (Figure 5). The *mt*CBS-PPase enzyme was gradually inactivated at pH 5. However, activity increased markedly with time at pH 7.2, and less markedly at pH 9. The extent of substrate conversion was < 5% in these experiments, and substrate effects therefore do not explain the nonlinearity. In contrast, progress curves were linear beyond the dead time of the phosphate analyzer (2 s) for *Escherichia coli* PPase devoid of CBS domains (Figure 5). The time courses of PP_i hydrolysis were described well by eqs 10 and 11, allowing estimation of the first-order rate constant for transition (k) as well as the initial (A_0) and final (A_{lim}) activities. A perfect fit was obtained in most cases, with a mean deviation of < 1% between the measured and calculated product concentrations.

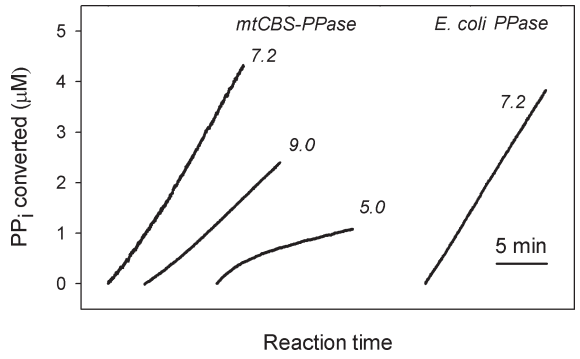

FIGURE 5: Time course of hydrolysis of PP_i by *mt*CBS-PPase at pH 5, 7.2, and 9 and *E. coli* PPase at pH 7.2. The assay medium contained 5 mM $MgCl_2$, 0.1 mM $CoCl_2$, and 8150 μM (pH 5), 160 μM (pH 7.2), or 140 μM (pH 9) PP_i, resulting in a Mg_2PP_i concentration of 100 μM. The reaction was initiated by addition of *mt*CBS-PPase or *E. coli* PPase to a final concentration of 40 or 0.4 ng/mL, respectively. Stock enzyme solutions of *mt*CBS-PPase (370 μg/mL) or *E. coli* PPase (3 μg/mL) were pre-equilibrated at 25 °C. Curve labels refer to enzyme identity and assay pH.

PP_i, Co^{2+}, and Mg^{2+} appeared to be absolutely required for activity transition. Thus, addition of PP_i and *mt*CBS-PPase in the reverse order (enzyme first followed by substrate after 15 min) did not significantly alter the progress curve at pH 7.2 (data not shown), indicating that no transitions had occurred during preincubation with Co^{2+} and Mg^{2+} in the absence of PP_i. Similarly, preincubation of *mt*CBS-PPase with PP_i in the absence of Co^{2+} and Mg^{2+}, the subsequent addition of which initiated the enzymatic reaction, did not affect the P_i production curve. Upon omission of Co^{2+} from enzyme storage and assay media, Mg^{2+}-supported activity was only ~1% of that supported by Mg^{2+} with Co^{2+}, but importantly, the product formation curve was strictly linear. Similarly, when Mg^{2+} was omitted from both enzyme storage and assay media, Co^{2+}-supported activity was 5% of that supported by Mg^{2+} with Co^{2+}, again with a linear product formation curve.

In view of the results obtained in the preincubation experiments, it is unlikely that the activity transition during the assay occurs because of a change in enzyme oligomeric structure triggered by dilution into assay medium. Further support for this assumption is offered by the finding that variations in stock enzyme concentration over the range of 1−100000 nM did not result in significant changes in the P_i production curve measured at pH 7.2.

Effects of Substrate and H^+ on the Activity Transition. Values of k, A_0, and A_{lim} changed in parallel upon variation of substrate (Mg_2PP_i) concentration at pH 5 and 7.2 (Figure 6). Similar dependencies were evident at pH 5.5 and 8.0. Dependencies were adequately described by the Michaelis−Menten equation, yielding the limiting values for each parameter and the K_m values listed in Table 4. At pH 5, A_{lim} values were too imprecise to permit measurement. K_m values derived from k, A_0, and A_{lim} dependencies were similar, within the errors of measurement, at fixed pH values. These results support the theory that activity transition occurs only in a productive enzyme−substrate complex and rule out a possibility that this effect results from a slow substrate binding step. With the latter mechanism, the value of k would increase linearly with substrate concentration. Furthermore, the slow substrate binding mechanism cannot explain the gradual decrease in activity observed at pH 5 (Figure 5).

The effects of assay pH on the values of k, A_0, and A_{lim} extrapolated to saturating substrate concentrations were moderate. A_0 and A_{lim} dependencies were bell-shaped, with pH optima at neutrality (Table 4). The k value increased monotonically with a decrease in pH. However, it is important to bear in mind that this parameter refers to inactivation at low pH and activation at high pH; that is, the directions of reaction are opposite, which complicates the interpretation of this parameter over the whole pH range.

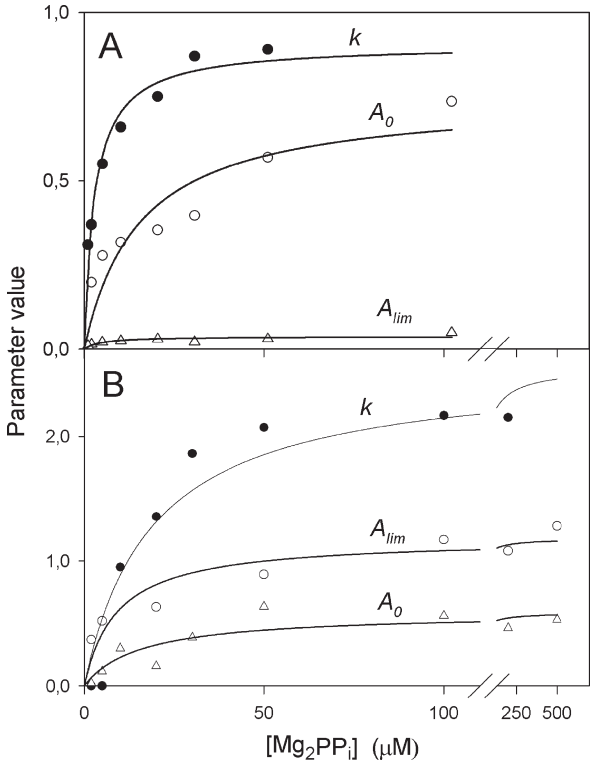

FIGURE 6: Dependence of k, A_0, and A_{lim} for the activity transition of *mt*CBS-PPase on substrate concentration at pH 5.0 (A) and 7.2 (B) measured with 5 mM Mg^{2+} and 0.1 mM $CoCl_2$. Values of k have units of inverse minutes and A_0 and A_{lim} inverse seconds. The lines represent the best fits for a simple hyperbolic function.

Table 4: Kinetic Parameters for the Activity Transition Derived from Substrate Concentration Dependencies of k, A_0, and A_{lim}

pH	dependence analyzed	p_{lim}[a]	K_m (μM)
5.0	k	1.3 ± 0.2	1.3 ± 1.2
5.0	A_0	0.57 ± 0.06	7 ± 3
5.0	A_{lim}	≤0.05	
7.2	k	1.8 ± 0.2	9 ± 1
7.2	A_0	1.3 ± 0.1	15 ± 7
7.2	A_{lim}	2.2 ± 0.2	8 ± 3
8.0	k	2.6 ± 0.9	6 ± 1
8.0	A_0	1.05 ± 0.01	24 ± 18
8.0	A_{lim}	2.05 ± 0.01	13 ± 3
8.5	k	2.8 ± 0.2	2 ± 1
8.5	A_0	0.38 ± 0.05	16 ± 5
8.5	A_{lim}	0.90 ± 0.03	9 ± 3

[a]Limiting value of respective parameters at an infinite substrate concentration. p_{lim} has units of inverse minutes (k dependence) or inverse seconds (A_0 and A_{lim} dependencies).

Effect of AMP on the Activity Transition. AMP added to assay medium induced decreases in both A_0 and A_{lim} (Figure 7A) and slowed the transition by decreasing k (Figure 7B). Interestingly, the limiting value of A_0 at infinite concentrations of AMP exceeded that of A_{lim} (Table 5), changing the transition effect

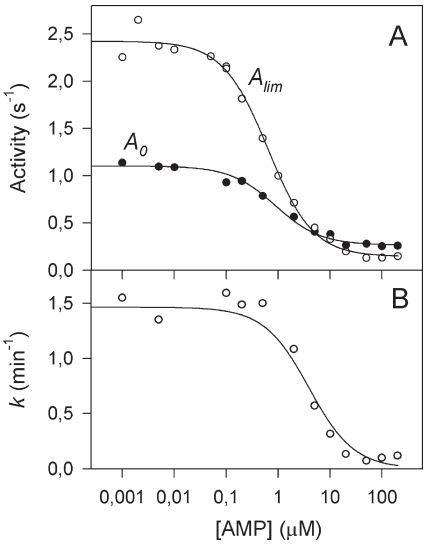

FIGURE 7: Dependence of k, A_0, and A_{lim} for the activity transition of *mt*CBS-PPase at pH 7.2 on AMP concentration. The substrate (Mg_2PP_i) concentration was 100 μM, while those of the cofactors were 5 mM Mg^{2+} and 0.1 mM $CoCl_2$. The lines represent the best fit for the equation, similar to eq 7.

Table 5: Parameter Values Describing AMP Dependencies of A_0, A_{lim}, and k in Figure 8

dependence analyzed	p_0[a]	p_{lim}[b]	K_i (μM)
k	1.5 ± 0.1	< 0.05	4 ± 1
A_0	1.2 ± 0.1	0.29 ± 0.02	0.9 ± 0.1
A_{lim}	2.0 ± 0.1	0.12 ± 0.03	0.6 ± 0.1

[a]Limiting values of respective parameters without AMP. [b]Limiting values of respective parameters at an infinite AMP concentration. p_0 and p_{lim} have units of inverse minutes (k dependence) or inverse seconds (A_0 and A_{lim} dependencies).

from 2-fold activation in the absence of AMP to 2-fold inactivation. The k value appeared to approach zero at saturating AMP concentrations. The K_i values governing the effects of AMP on A_0 and A_{lim} (Table 5) were similar to the K_{d2} obtained in fluorescence titrations (Table 1). In contrast, k analysis yielded a significantly higher K_i value of 4 μM, which is closer to K_{d2} (Table 1).

Finally, preincubation of a 10 μM stock enzyme solution with 100 μM AMP for 3 h did not affect the PP_i hydrolysis curve, indicating that the enzyme states induced by PP_i and AMP are distinct. In the case of identical PP_i hydrolysis curves, the AMP-preincubated enzyme would produce a linear reaction time course, with the slope corresponding to A_{lim}.

Kinetic Titration of Nucleotide-Binding Sites. ADP binds tightly to *mt*CBS-PPase (K_d = 0.01 μM), with concomitant inhibition of enzyme activity (*8*). As *mt*CBS-PPase is only moderately active (k_{cat} = 1.7 s^{-1}) (*8*), this allows estimation of the ADP binding stoichiometry from activity measurements. Thus, 10 μM enzyme was allowed to react for 30 s with 100 μM PP_i in the presence of variable concentrations of ADP. Nearly 80% of PP_i was consumed in the absence of ADP, and control experiments indicated that hydrolysis proceeded linearly with time under these conditions. Figure 8 shows a sharp inflection point at 0.33 mol of ADP/mol of enzyme. For different enzyme preparations, this value was in the range of 0.10−0.33 mol/mol. Our findings suggest that the smaller population of *mt*CBS-PPase

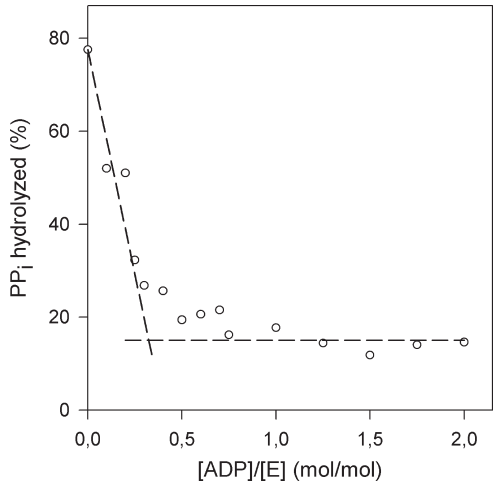

FIGURE 8: Kinetic titration based on ADP binding sites in *mt*CBS-PPase. The dashed lines represent tangents to the initial and final parts of the dependence. The abscissa of the intersection point (0.33 mol/mol) corresponds to the ADP binding stoichiometry.

is more sensitive to ADP inhibition and has higher activity compared with the larger population. On the basis of the coordinates of the inflection point, the specific activities of the two enzyme populations should differ by a factor of ~10.

DISCUSSION

Conformational Flexibility of mtCBS-PPase. Activity transitions resulting in nonlinear reaction time courses indicate that *mt*CBS-PPase adopts at least two conformations with different activities. This theory is strongly supported by ADP titration data (Figure 8) showing that binding of only 0.33 molecule of ADP per active site is sufficient for inhibition of the bulk of activity. The results imply that only one-third of the enzyme in a stock solution is present in the more active conformation (H-conformation), with the remaining two-thirds in a less active conformation (L-conformation). In this respect, *mt*CBS-PPase is similar to another CBS domain-containing protein, endosomal Cl^-/H^+ antiporter ClC-5, which can also exist as both active and inactive forms in the absence of nucleotides (*28*). Specific activities of the H- and L-conformations of *mt*CBS-PPase are estimated to differ by a factor of 10. In view of these estimates, full conversion of the enzyme into the H-conformation would increase activity by a factor of 2.5, close to the A_{lim}/A_0 value for the substrate-induced activity transition in alkaline medium (Table 4). At pH 5, the H-conformation appears to be less active than the L-conformation. Alternatively, the transition may occur in the opposite direction, that is, from the H- to the L-conformation, at pH 5. ADP titration data additionally show that the L-conformation has a significantly lower affinity for ADP. This additionally applies to AMP binding, as estimated from effects of AMP on A_{lim} and k (Table 5), although differences in binding constants are markedly lower for AMP.

Mant-AMP also affects *mt*CBS-PPase conformation. These changes are resolved into three steps in stopped-flow analysis. The slowest step occurs with a transit time of 16−280 s, depending on Mant-AMP concentration (Table 2), similar to that of substrate-induced conformational changes (30−40 s transit time). However, nucleotide-induced conformational changes do not lead to the transition of A_0 to A_{lim} and therefore differ from the substrate-induced ones. Nevertheless, the active and regulatory sites are tightly connected, and this is evident from the

effects of bound nucleotides on enzymatic activity, and PP_i on nucleotide-induced transitions.

Notably, *mt*CBS-PPase contains only two Trp residues per subunit, at positions 128 and 295. On the basis of the X-ray structure of *C. perfringens* PPase, Trp128 (conserved in PPases) is ~20 Å from bound AMP, whereas Trp295 (nonconserved) appears to be much more distant. Clearly, Trp128 is involved in fluorescence resonance energy transfer to bound Mant-AMP in *mt*CBS-PPase. The residue is located in the boundary between CBS and the catalytic domains and should be highly sensitive to structural changes in both regulatory and active sites. As energy transfer strongly depends on the mutual orientation of Trp and Mant-AMP, this pairing represents a unique method for probing the *mt*CBS-PPase structure. Interestingly, the binding step per se generated little fluorescence, suggesting that either the distance between Trp128 and Mant-AMP is much larger in the initial complex or their mutual orientation is unfavorable for energy transfer. The finding that nucleotides induce conformational changes in *mt*CBS-PPase is supported by the effects of AMP on binding of the hydrophobic dyes, 8-anilinonaphthalene 1-sulfonate and Nile Red, to the enzyme (data not shown).

Nucleotide Binding Sites. Initial evidence of the presence of two types of nucleotide binding sites, with different affinities, in *mt*CBS-PPase was obtained from fluorescence titration data and supported by results of stopped-flow measurements. In addition to the site with a K_d value of approximately 10 μM, which controls the transit times and amplitudes of fluorescence signals (Table 2), there should also be a site responsible for the appearance of such signals. As neither transit time decreases with an increase in Mant-AMP concentration (Figure 3A), it appears that this site binds Mant-AMP at a rate faster than what can be resolved using the stopped-flow method. Furthermore, the site becomes nearly or completely saturated, even at the lowest Mant-AMP concentration employed (8 μM). Accordingly, the K_d value for this site is ≤ 1 μM. In view of the fluorescence titration data (Table 1), the site characterized by K_{d1} is the optimal candidate and appears to be the inhibitory site, based on comparison of K_d (Table 1) and K_i (Table 5) values. It is important to consider that the K_i values obtained from inhibition measurements (Table 5) are the upper limits of true K_d values, as the substrate, essentially present during these measurements, binds competitively (*8*). A logical corollary is that the K_{d2} value obtained from direct binding measurements with Mant-AMP (Table 1) belongs to the modulatory site, which affects both nucleotide-induced (Table 3) and substrate-induced (Table 5) conformational transitions.

The existence of two binding sites with different affinities in a homodimeric protein cannot be reconciled with a binding stoichiometry of ~1 mol/mol of subunit obtained by direct binding measurements unless one assumes some kind of enzyme asymmetry (i.e., a negative binding cooperativity). If all sites bind Mant-AMP independently, the binding stoichiometry would be 2 mol/mol at the nucleotide concentrations used to produce the data of Figure 4. The simplest mechanism explaining our data assumes that dimeric *mt*CBS-PPase has two initially identical nucleotide binding sites, but binding to one of the sites induces a change in the structure of the other, thus decreasing its affinity. In the *C. perfringens* PPase structure, the AMP binding sites (one per subunit) are located near the subunit interface, in the proximity of each other. The distance between bound AMP molecules is only 9 Å, leading to an increased possibility of interactions in the binding reaction. After binding of the second nucleotide, the symmetry of the structure is restored. The transitions characterized by τ_0 and τ_{lim} thus refer to structural changes inducing asymmetry and restoring symmetry, respectively. Within the framework of this mechanism, Mant-AMP bound at the "modulatory" site does not greatly modulate the emission of light from Mant-AMP bound at the other site. Accordingly, the fluorescence level increases when the second site is occupied (Figure 1).

In summary, nucleotides induce conformational changes in *mt*CBS-PPase, occurring in several steps over a wide time scale and differing from substrate-induced conformational changes. These findings aid in improving our knowledge of the mechanism(s) underlying the regulatory roles of CBS domains in *mt*CBS-PPase and numerous other proteins. Further clarification of the detailed mechanism(s) will require determination of a repertoire of protein structures with different bound nucleotide contents.

REFERENCES

1. Kornberg, A. (1962) On the metabolic significance of phosphorolytic and pyrophosphorolytic reactions. In Horizons in Biochemistry (Kasha, M., and Pullman, B., Eds.) pp 251−264, Academic Press, New York.
2. Baykov, A. A., Cooperman, B. S., Goldman, A., and Lahti, R. (1999) Cytoplasmic inorganic pyrophosphatases. *Prog. Mol. Subcell. Biol. 23*, 127–150.
3. Merckel, M. C., Fabrichniy, I. P., Salminen, A., Kalkkinen, N., Baykov, A. A., Lahti, R., and Goldman, A. (2001) Crystal structure of *Streptococcus mutans* pyrophosphatase: a new fold for an old mechanism. *Structure 9*, 289–297.
4. Ahn, S., Milner, A. J., Fütterer, K., Konopka, M., Ilias, M., Young, T. W., and White, S. A. (2001) The "open" and "closed" structures of the type-C inorganic pyrophosphatases from *Bacillus subtilis* and *Streptococcus gordonii*. *J. Mol. Biol. 313*, 797–811.
5. Bateman, A. (1997) The structure of a domain common to archaebacteria and the homocystinuria disease protein. *Trends Biochem. Sci. 22*, 12–13.
6. Scott, J. W., Hawley, S. A., Green, K. A., Anis, M., Stewart, G., Scullion, G. A., Norman, D. G., and Hardie, D. G. (2004) CBS domains form energy-sensing modules whose binding of adenosine ligands is disrupted by disease mutations. *J. Clin. Invest. 113*, 274–284.
7. Ignoul, S., and Eggermont, J. (2005) CBS domains: structure, function, and pathology in human proteins. *Am. J. Physiol. 289*, C1369–C1378.
8. Jämsen, J., Tuominen, H., Salminen, A., Belogurov, G. A., Magretova, N. N., Baykov, A. A., and Lahti, R. (2007) A CBS domain-containing pyrophosphatase of *Moorella thermoacetica* is regulated by adenine nucleotides. *Biochem. J. 408*, 327–333.
9. Carr, G., Simmons, N., and Sayer, J. (2003) A role for CBS domain 2 in trafficking of chloride channel ClC-5. *Biochem. Biophys. Res. Commun. 310*, 600–605.
10. Bieman-Oldehinkel, E., Mahmood, N. B. N., and Poolman, B. (2006) A sensor for intracellular ionic strength. *Proc. Natl. Acad. Sci. U.S.A. 103*, 10624–10629.
11. Mahmood, N. A., Biemans-Oldehinkel, E., and Poolman, B. (2009) Engineering of ion sensing by the cystathionine β-synthase module of the ABC transporter OpuA. *J. Biol. Chem. 284*, 14368–14376.
12. Ishitani, R., Sugita, Y., Dohmae, N., Furuya, N., Hattori, M., and Nureki, O. (2008) Mg^{2+}-sensing mechanism of Mg^{2+} transporter MgtE probed by molecular dynamics study. *Proc. Natl. Acad. Sci. U.S.A. 105*, 15393–15398.
13. De Angeli, A., Moran, O., Wege, S., Filleur, S., Ephritikhine, G., Thomine, S., Barbier-Brygoo, H., and Gambale, F. (2009) ATP binding to the C-terminus of the *Arabidopsis thaliana* nitrate/proton antiporter, AtCLCa, regulates nitrate transport into plant vacuoles. *J. Biol. Chem. 284*, 26526–26532.
14. Pimkin, M., Pimkina, J., and Markham, G. D. (2009) A regulatory role of the Bateman domain of IMP dehydrogenase in adenylate nucleotide biosynthesis. *J. Biol. Chem. 284*, 7960–7969.
15. Zhang, R., Evans, G., Rotella, F. J., Westbrook, E. M., Beno, D., Huberman, E., Joachimiak, A., and Collart, F. R. (1999) Characteristics and crystal structure of bacterial inosine-5′-monophosphate dehydrogenase. *Biochemistry 38*, 4691–4700.

16. Miller, M. D., Schwarzenbacher, R., von Delft, F., Abdubek, P., Ambing, E., Biorac, T., Brinen, L. S., Canaves, J. M., Cambell, J., Chiu, H. J., Dai, X., Deacon, A. M., DiDonato, M., Elsliger, M. A., Eshagi, S., Floyd, R., Godzik, A., Grittini, C., Grzechnik, S., Hampton, E., Jaroszewski, L., Karlak, C., Klock, H. E., Koesema, E., Kovarik, J. S., Kreusch, A., Kuhn, P., Lesley, S. A., Levin, I., McMullan, D., McPhillips, T. M., Morse, A., Moy, K., Ouyang, J., Page, R., Quijano, K., Robb, A., Spraggon, G., Stevens, R. C., van den Bedem, H., Velasquez, J., Vincent, J., Wang, X., West, B., Wolf, G., Xu, Q., Hodgson, K. O., Wooley, J., and Wilson, I. A. (2004) Crystal structure of a tandem cystathionine-β-synthase (CBS) domain protein (TM0935) from *Thermotoga maritima* at 1.87 Å resolution. *Proteins 57*, 213–217.
17. Meyer, S., and Dutzler, R. (2006) Crystal structure of the cytoplasmic domain of the chloride channel ClC-0. *Structure 14*, 299–307.
18. Hattori, M., Tanaka, Y., Fukai, S., Ishitani, R., and Nureki, O. (2007) Crystal structure of the MgtE Mg^{2+} transporter. *Nature 448*, 1072–1075.
19. Jin, X., Townley, R., and Shapiro, L. (2007) Structural insight into AMPK regulation: ADP comes into play. *Structure 15*, 1285–1295.
20. Proudfoot, M., Sanders, S. A., Singer, A., Zhang, R., Brown, G., Binkowski, A., Xu, L., Lukin, J. A., Murzin, A. G., Joachimiak, A., Arrowsmith, C. H., Edwards, A. M., Savchenko, A. V., and Yakunin, A. F. (2008) Biochemical and structural characterization of a novel family of cystathionine β-synthase domain proteins fused to a Zn ribbon-like domain. *J. Mol. Biol. 375*, 301–315.
21. Ragunathan, P., Kumarevel, T., Agari, Y., Shinkai, A., Kuramitsu, S., Yokoyama, S., and Ponnuraj, K. (2008) Crystal structure of ST2348, a CBS domain protein, from hyperthermophilic archaeon *Sulfolobus tokodaii*. *Biochem. Biophys. Res. Commun. 375*, 124–128.
22. King, N. P., Lee, T. M., Sawaya, M. R., Cascio, D., and Yeates, T. O. (2008) Structures and functional implications of an AMP-binding cystathionine β-synthase domain protein from a hyperthermophilic archaeon. *J. Mol. Biol. 380*, 181–192.
23. Pace, C. N., Vajdos, F., Fee, L., Grimsley, G., and Gray, T. (1995) How to measure and predict the molar absorption coefficient of a protein. *Protein Sci. 4*, 2411–2423.
24. Jones, L. J., Haugland, R. P., and Singer, V. L. (2003) Development and characterization of the NanoOrange protein quantitation assay: A fluorescence-based assay of proteins in solution. *BioTechniques 34*, 850–854.
25. Baykov, A. A., and Avaeva, S. M. (1981) A simple and sensitive apparatus for continuous monitoring of orthophosphate in the presence of acid-labile compounds. *Anal. Biochem. 116*, 1–4.
26. Tonomura, B., Nakatani, H., Ohnishi, M., Yamaguchi-ito, J., and Hiromi, K. (1978) Test reactions for a stopped-flow apparatus. Reduction of 2,6-dichlorophenoiindophenol and potassium ferricyanide by L-ascorbic acid. *Anal. Biochem. 84*, 370–383.
27. Hiratsuka, T. (1983) New ribose-modified fluorescent analogs of adenine and guanine nucleotides available as substrates for various enzymes. *Biochim. Biophys. Acta 742*, 496–508.
28. Zifarelli, G., and Pusch, M. (2009) Intracellular regulation of human ClC-5 by adenine nucleotides. *EMBO Rep. 10*, 1111–1116.